



# Distribution of Cambrian Source Rock Controlled by the Inherited Paleotopography on the Precambrian Basement in the Tarim Basin, NW China

Haowei Yuan<sup>1,2</sup>, Shuping Chen<sup>1,2\*</sup>, Kun Dai<sup>3</sup>, Xiaochen Guo<sup>4</sup>, Linghua Kong<sup>5</sup>, Nana Feng<sup>6</sup>, Huaibo Zhao<sup>1,2</sup> and Weili Yang<sup>7</sup>

<sup>1</sup>State Key Laboratory of Petroleum Resources and Prospecting, China University of Petroleum (Beijing), Beijing, China, <sup>2</sup>College of Geosciences, China University of Petroleum (Beijing), Beijing, China, <sup>3</sup>CNPC Engineering Technology R&D Company Ltd., Beijing, China, <sup>4</sup>Engineering Company of CNPC Bohai Drilling Engineering Branch Company Limited, Bohai, China, <sup>5</sup>PetroChina Xinjiang Oilfield Company, Xinjiang, China, <sup>6</sup>Exploration and Development Research Institute PetroChina Huabei Oilfield Company, Huabei, China, <sup>7</sup>SINOPEC Petroleum Exploration and Production Research Institute, Beijing, China

## OPEN ACCESS

### Edited by:

Shu Jiang,

The University of Utah, United States

### Reviewed by:

Wen Zhiang,

China University of Geosciences,

China

Ruyue Wang,

SINOPEC Petroleum Exploration and

Production Research Institute, China

Chen Zhang,

Chengdu University of Technology,

China

Jie Xu,

Goethe University Frankfurt, Germany

### \*Correspondence:

Shuping Chen

csp21c@163.com

### Specialty section:

This article was submitted to

Structural Geology and Tectonics,

a section of the journal

Frontiers in Earth Science

Received: 28 January 2022

Accepted: 29 April 2022

Published: 13 June 2022

### Citation:

Yuan H, Chen S, Dai K, Guo X, Kong L,

Feng N, Zhao H and Yang W (2022)

Distribution of Cambrian Source Rock

Controlled by the Inherited

Paleotopography on the Precambrian

Basement in the Tarim Basin,

NW China.

Front. Earth Sci. 10:864082.

doi: 10.3389/feart.2022.864082

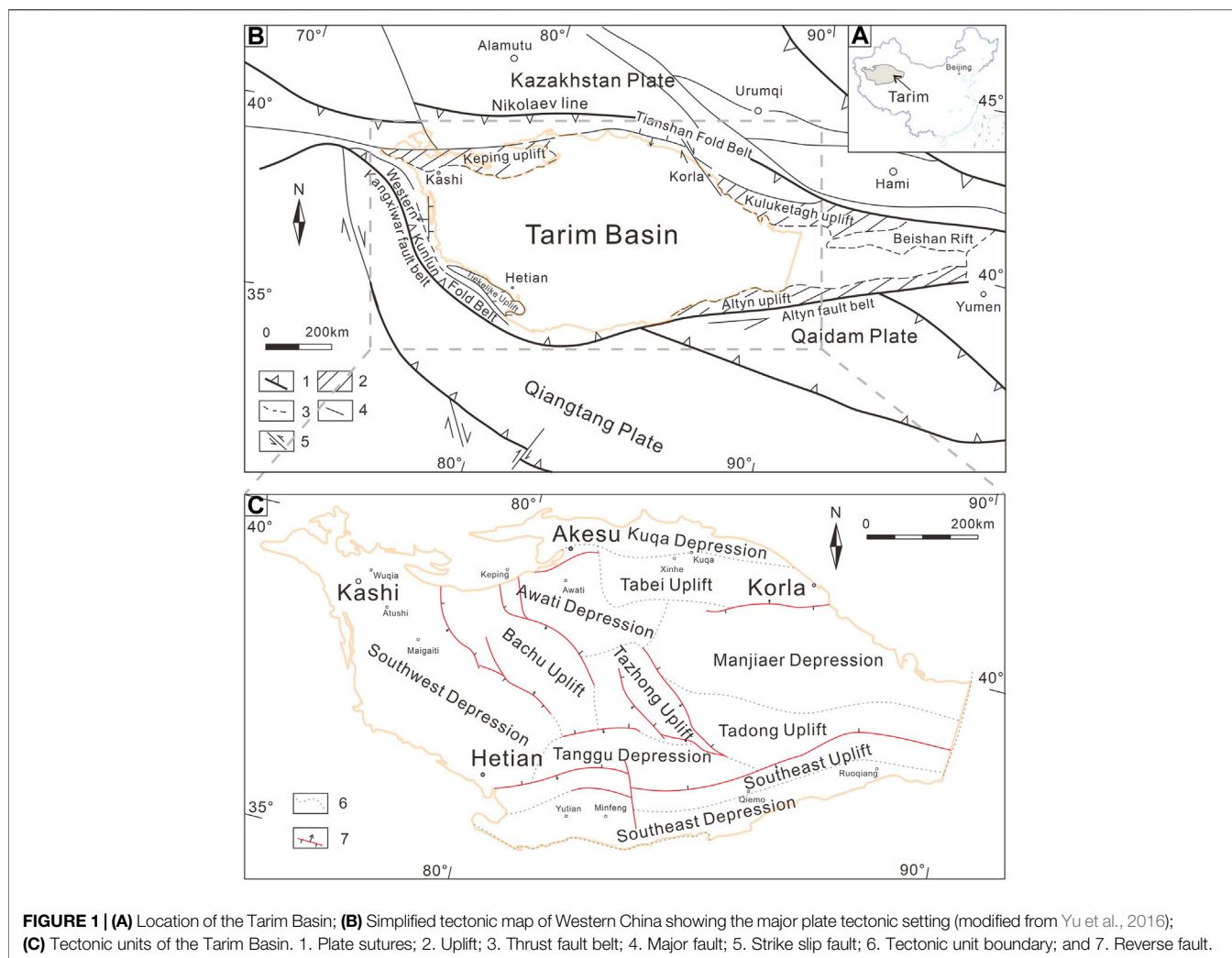
The Cambrian source rock is a key indicator that will guide future hydrocarbon explorations in ultra-deep strata. Despite its importance, the characteristics of paleotopography on the Precambrian basement and the distribution of source rocks above it remain unclear. The seismic and borehole data, isopach data, and the unconformity analysis are used to study the relations of the Cambrian source rock distribution to the paleotopography. The consistency of the strata thickness distribution maps of the Nanhua–Cambrian sequences show that the extensive thermal subsidence lasted the whole Sinian period, and makes the paleotopography of the Precambrian basement inherited from the landform after the Nanhua continental rifting. A major transgression caused by rapid subsidence of the Tarim Basin took place during the Cambrian. Shales were deposited offshore along the slopes of a paleo-uplift on the inherited paleotopography and formed the onlap in seismic profiles. The onlap on the inherited paleotopography reflects the distribution range of Yuertusi source rocks in the Cambrian.

**Keywords:** tarim basin, neoproterozoic, cambrian, onlap unconformity, rifting, thermal subsidence, source rock

## INTRODUCTION

The Tarim Basin is located in northwestern China (**Figure 1A**) and is the third-largest petroliferous basin in China (He et al., 1998). It has undergone numerous episodes of complex and multi-stage tectonic movements (Yu et al., 2016; Jin et al., 2017). The Sinian–Cambrian system includes important petroleum plays. However, because this system is deeply buried, the distribution of source rocks and reservoirs remains controversial (Xu et al., 2013; Zhu et al., 2018; Yang et al., 2020). The palaeomorphology has a great geological significance because it is controlled by the Neoproterozoic tectonic evolution and it has considerably influenced the distribution of the Lower Cambrian source rock in the Tarim Basin. Furthermore, the Cambrian source rock is a key indicator that will guide future hydrocarbon explorations in ultra-deep strata (Zhu et al., 2016; Zhu et al., 2018).

Whether or not the Cambrian source rock distribution is possibly due to the effect of inherited structures is a current debate (Zhu et al., 2018; Yang et al., 2020). Whether the formation of inherited



paleotopography on the Precambrian basement has been continuously deposited, eroded, or bypassed is a subject of debate. Some studies have found that the deposition occurred in an extensional tectonic setting in the Tarim Basin (Jia, 1997; He et al., 1998; Zhou et al., 2012). However, observations of the stratal truncations in seismic data (see below) suggest that an unconformity exists between the Sinian and the Cambrian intervals, implying that erosion existed from the Sinian to the Cambrian intervals (Wu et al., 2012; Yan et al., 2018). In order to address these issues, it is important to understand the tectonic evolution of the Nanhua–Cambrian system and the relations of onlap on the inherited paleotopography to the Cambrian source rock.

With these in mind, we used the seismic and well data, lithology and stratigraphy data to study the formation and properties of the paleotopography. The contact relations between the Sinian and Cambrian were determined by analyzing structures of the Neoproterozoic basin and by comparing the thickness of the lower Cambrian Yuertusi Formation with those of the Neoproterozoic strata. And we developed the onlap type on the paleotopography to study the distribution of the source rocks in the lower Cambrian.

## GEOLOGICAL SETTING

The Tarim Basin is located in the Xinjiang Uygur Autonomous Region, China (Figure 1). The basin covers an area of  $5.6 \times 10^5 \text{ km}^2$  and is bounded by the Tianshan fold belt, Kunlun fold belt, and Altyn fault zone. Four sets of source rocks have been identified in the basin: lower Cambrian, upper–middle Ordovician, Carboniferous–Permian, and Triassic–Jurassic rocks (e.g., He et al., 1998; Jin and Wang, 2004; Lu et al., 2020; Tang et al., 2006; Cai, 2007; Gao and Fan, 2015; Wu et al., 2016). Among these, the black shales of the Yuertusi Formation at the base of the lower Cambrian (Figure 2) have attracted interest as potential sources of petroleum for the deep Neoproterozoic, Cambrian, and possibly Ordovician reservoirs (Gao and Fan, 2015; Zhu et al., 2016).

### Tectonic Setting of the Tarim Basin

The Tarim Basin is composed of Pre-Neoproterozoic metamorphic basement rocks overlain by sedimentary rocks of the Neoproterozoic–Cenozoic age (He et al., 2006; Feng et al., 2015; Jiang et al., 2016). The Kazakhstan and Siberian plates are

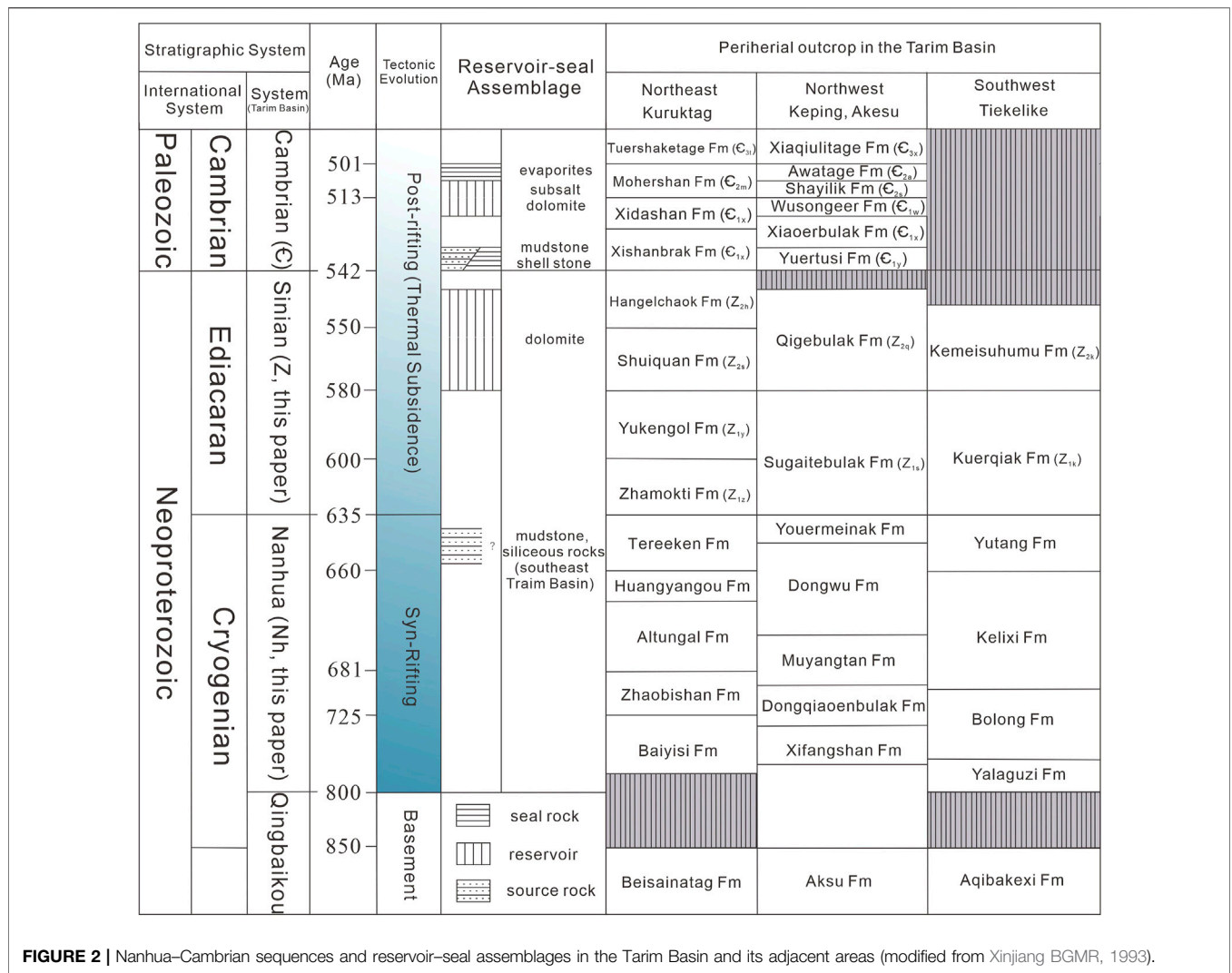


**FIGURE 2 |** Nanhua–Cambrian sequences and reservoir–seal assemblages in the Tarim Basin and its adjacent areas (modified from Xinjiang BGMR, 1993).

located to the north, the Chaidamu Plate to the southeast, and the Qiangtang Plate to the south (Figure 1B). The inner Tarim Basin is divided into the Southwest Depression, Tanguzibasi Depression, Bachu Uplift, Tazhong Uplift, Awati Depression, Manjiaer Depression, Tabei Uplift, Southeast Uplift, and Southeast Depression (He et al., 2006; Zhang et al., 2013; Yu et al., 2016; Figure 1C).

The collision of the northern margin of the Tarim Plate with the Kazakhstan Plate formed the Tianshan fold belt during the late Paleozoic. The Kunlun fold belt is located at the southwestern margin of the Tarim Plate, and the Kangxiwar fault belt is adjacent to the northern margin of Kunlun. The Kangxiwar suture zone forms the southwestern boundary of the Tarim Plate (Yu et al., 2016; Figure 1B), while the Altyn fault belt, a large strike-slip fault active during the Mesozoic and Cenozoic ages, forms the boundary between the Tarim Basin and the Qaidam Plate (Ren et al., 1999; Figure 1B).

The Tarim Basin developed on the pre-Nanhua continental metamorphic basement (Ge et al., 2016), and has subsequently undergone three primary extension–convergence cycles during

its tectonic evolution. These cycles have lasted from the Neoproterozoic (Nanhua) to the Middle Devonian, from the Late Devonian to the Permian, and from the Mesozoic to the Cenozoic (He et al., 2016). Particularly in the Cenozoic, the collision between the Indian and Eurasian Plates caused thrusting, strike–slip, and compression in the Tarim Basin and adjacent regions (Li et al., 2010; Xu et al., 2013; Xu et al., 2013; Zhang et al., 2013; Yu et al., 2016).

### Nanhua-Cambrian Stratigraphy

The Nanhua and Sinian sequences are exposed in the Tiekelike, Keping, and Kuruktag areas along the southwestern, northwestern, and northeastern margins of the Tarim Basin, respectively (Xu et al., 2009; Turner, 2010; Figure 2). The Nanhua strata primarily consist of clastic rocks of littoral-neritic facies, tillite rocks of glacial facies, and volcanic rocks. In the Kuruktag area, the volcanic rocks of the Nanhua intervals consist of tuff, basalt, and rhyolite. Moreover, mafic dykes exist in the Nanhua strata in Well YL1 (Figure 3), all of which are indicative of continental rifting (Zhang et al., 2013; Yu et al.,

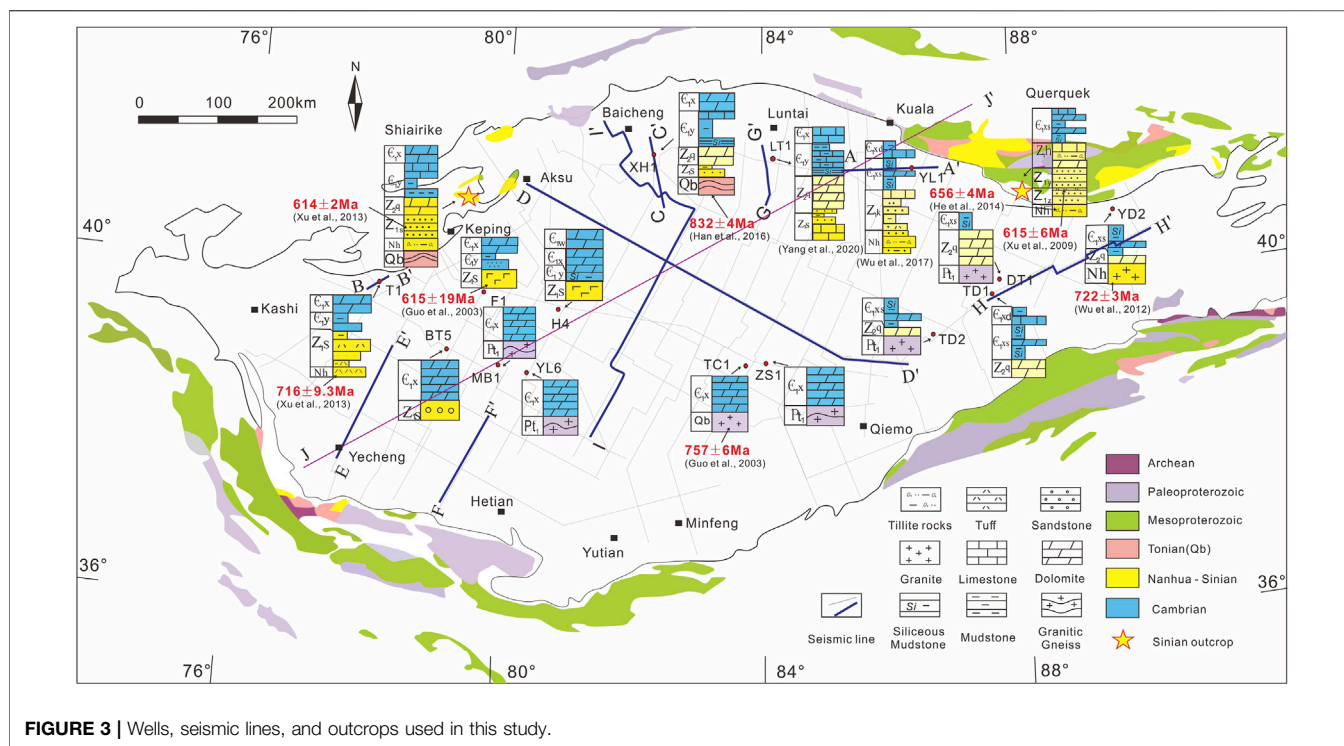


FIGURE 3 | Wells, seismic lines, and outcrops used in this study.

2016). In the southwest zone, the Nanhua Formation includes the Yutang, Kelixi, Bolong, Yalaguzi formations, which have a combined thickness of 2,500 m.

The lower Sinian strata in the northern Tarim Basin consist of sandstones and mudstones deposited on the continental shelf. The lower Sinian in the southern Tarim Basin consists of deltaic facies rocks and carbonaceous detrital rocks. The differences in the sedimentary environments between the southern and northern parts of the Tarim Basin of the Upper Sinian gradually decrease with decreasing age. A carbonate-rich continental shelf facies is present in the northern Tarim Basin, whereas a dolomite tidal flat facies is present in the southern Tarim Basin (Feng et al., 2015; Shi et al., 2016; Wu et al., 2016; Zhang et al., 2019). Previous scholars have used the U–Pb zircon age to determine the ages of the Nanhua–Sinian strata in the wells of the Tarim Basin. In Well T1, Neoproterozoic pyroclastic rocks have a U–Pb zircon age of  $716 \pm 9.3$  Ma, which is the age of the Dongqiaoenbulak Formation in the Nanhua Formation (Xu et al., 2013). Similarly, the volcanic rocks of the Nanhua Formation from Well YD1 have a U–Pb zircon age of  $722 \pm 3$  Ma (Wu et al., 2012), very similar to those in Well T1 in the northwestern Tarim Basin. In the central Tarim Basin, the Lower Cambrian rocks in wells MB1, YL6, TC1, and ZS2 overlie the pre-Nanhua metamorphic basement, and the granitic gneiss in Well TC1 has a U–Pb zircon age of  $757 \pm 6$  Ma (Guo et al., 2003). In the northern Tarim Basin, Nanhua Formation rocks are missing in Well XH1, while the gneiss below the Sinian strata has a U–Pb zircon age of  $832 \pm 4$  Ma (Han et al., 2016).

Drilling data show that the Sinian sedimentary areas are overlain by the Cambrian Yuertusi Formation (Figure 3). The lower Yuertusi strata are composed of black mudstones and littoral–shallow marine

siliceous rocks. After the Sinian, a major transgression occurred (possibly due to rising sea levels), and the Cambrian succession in the eastern Tarim Basin exhibits an open platform facies and is mainly composed of marine carbonate rocks, sandstones, and mudstones (Luo, 1998; Shi et al., 2018; Zhang et al., 2019). There was no significant igneous activity during the Sinian–Cambrian, and in the southwest, the Cambrian strata are eroded.

The oil and gas reservoirs related to the lower Cambrian are designated as the lower hydrocarbon-bearing assemblage. These source rocks occur in the Nanhua–Sinian Formation and the Yuertusi Formation (Wu et al., 2016; Zhu et al., 2016). This lower hydrocarbon-bearing assemblage consists of two sets of regional reservoir and seal combinations. The Shayilik–Wusongeer Formation dolomite is sealed by evaporites (gypsum and halites) of the middle Cambrian Awatage Formation (Figure 2), and the upper Sinian Qigebulak Formation dolomite is sealed by the shale of the lower Cambrian Yuertusi Formation (Gao and Fan, 2015; Yang et al., 2020). The mudstone in the Yuertusi Formation is the highest-quality marine source rock, with a thickness of 15–40 m and a total organic carbon (TOC) content of 2–16% (Zhu et al., 2016). The mudstone in the Yuertusi Formation is a high-quality source rock for the upper reservoir and a seal rock for the lower reservoir (Luo et al., 2014; Zhu et al., 2016; Cui et al., 2017; Figure 2). Consequently, the distribution of the Yuertusi Formation is crucial for exploration in both the upper and lower hydrocarbon-bearing assemblages.

## DATA AND METHODS

The Exploration and Production Research Institute, SINOPEC, provided the 2D seismic reflection data. The seismic data covered

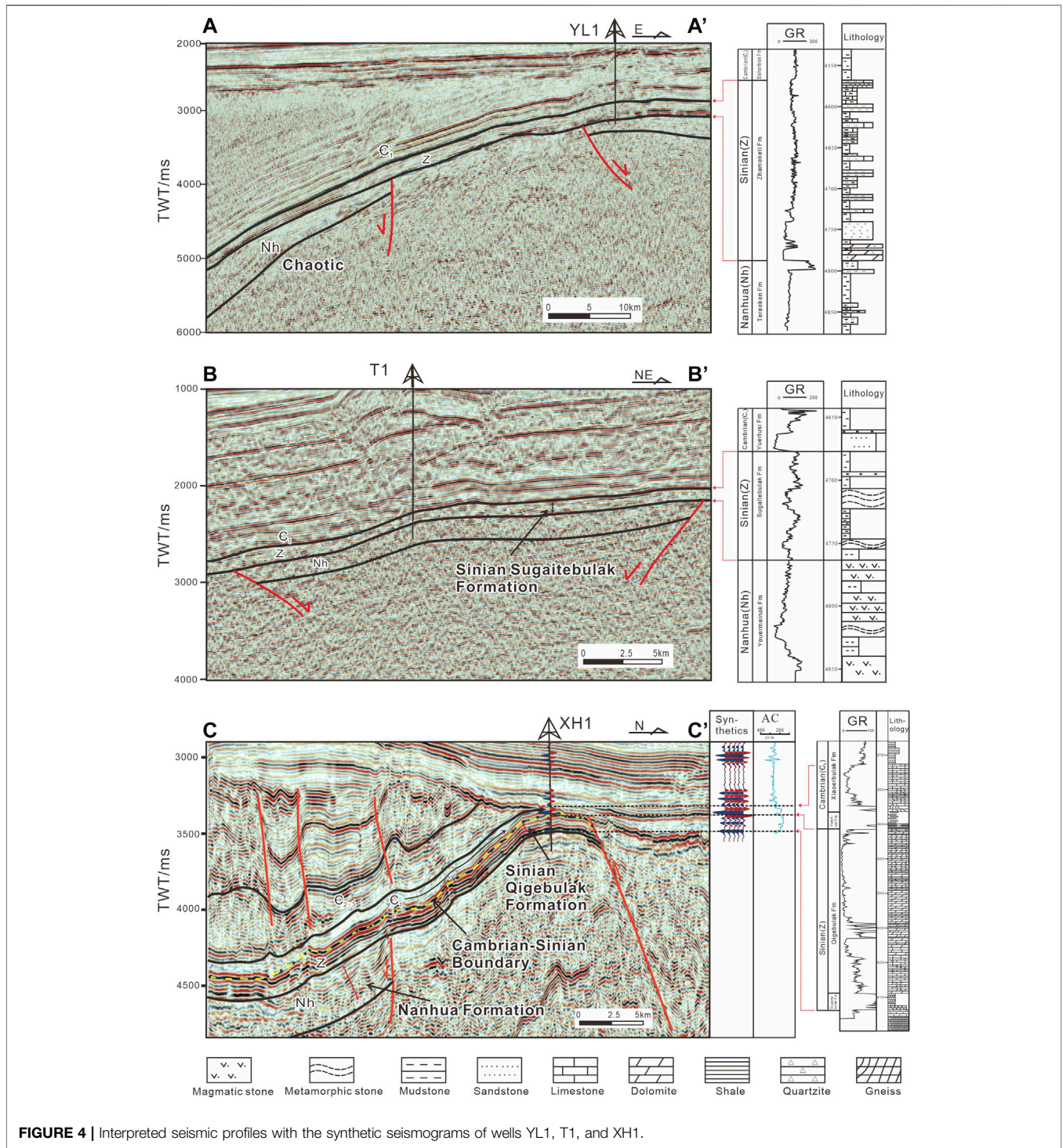


**FIGURE 4 |** Interpreted seismic profiles with the synthetic seismograms of wells YL1, T1, and XH1.

the entire Tarim Basin (area of  $1.4 \times 10^4$  km; **Figure 3**). These data were reprocessed using 2D pre-stack depth migration in 2017 by SINOPEC. Fifteen wells drilled into or through the Sinian or Nanhua strata (**Figures 3,4**) were used to calibrate the interpretation of the seismic data from the Nanhua–Sinian–Cambrian sedimentary sequences and the Middle–Late Proterozoic metamorphic

crystalline basement (**Table 1**). In addition, the thickness maps of the Nanhua, Sinian, and Cambrian strata were produced by petrel software after the seismic interpretation.

The seismic reflection terminations can be used to delineate unconformities and distinguish seismic facies units (Veeken, 2006). The seismo-stratigraphic data within the

**TABLE 1** | U-Pb zircon age data from the Tarim Basin.

Wells or outcrops	Formation	Age (Ma)	References
T1	Nanhua (Nh)	716 ± 9.3	Xu et al. (2013)
F1	Sinian (Z)	615 ± 19	Guo et al. (2003)
XH1	Tonian (Qb)	832 ± 4	Han et al. (2016)
TC1	Tonian (Qb)	757 ± 6	Guo et al. (2003)
TD2	Paleoproterozoic	1908 ± 9	Wu et al. (2012)
YD2	Nanhua (Nh)	722 ± 3	Wu et al. (2012)
Keping	Sinian (Z)	614 ± 2	Xu et al. (2013)
Kuluketage	Nanhua (Nh)	656 ± 4	He et al. (2016)
Kuluketage	Sinian (Z)	615 ± 6	Xu et al. (2009)

Neoproterozoic–Cambrian succession provides insight into the paleo-geomorphic and tectonic evolution of the Tarim Basin. Combined with well data (lithology, U–Pb zircon ages of rock cores, and logging curves), such as those from wells T1, YL1, and XH1 (**Figure 4**), the characteristics of the seismic reflectors can be determined.

## RESULT

### Seismic Stratigraphic Interpretation

The lower Cambrian Yuertusi Formation is composed of mudstones and siltstones, and typically displays parallel and continuous, high-frequency, and high-amplitude seismic reflections (**Figure 4C**). The upper Sinian Qigebulak Formation consists of dolomite and is characterized by mid-parallel and lower-continuous, low-frequency, and medium-amplitude reflections (**Figure 4A**). The lower Sinian Sugaitebulak Formation consists of sandstones, mudstones, tillites, and volcanic rocks and displays discontinuous, high-frequency, and medium-amplitude seismic reflections (**Figure 4B**). In the seismic data, the Cambrian–Sinian sequence boundary is seen as a very high-amplitude and continuous reflector, and the Cambrian sequence is seen as low-amplitude reflectors (**Figure 4C**). The Nanhua strata are predominantly composed of sandstones, mudstones, tillites, and clastic rocks, whose seismic facies units are similar to those of the lower Sinian strata. However, some areas exhibit layered seismic reflections. Both the Sinian and Nanhua Formations are easily distinguished from the Late Proterozoic metamorphic crystalline basement, displaying discontinuous and low-amplitude seismic reflections and chaotic seismic reflection units in some areas (i.e., profile A–A'; **Figure 4A**).

### Types of Unconformities on the Inherited Paleotopography

Types of unconformities reflect both the tectonic movements and the paleo-geomorphology in a region (McKenzie, 1978; Christie-Blick, 1991). Thinning and truncations in the seismic profiles of the base of the Cambrian intervals indicate unconformities in the basin. Three types of unconformities are observed on the inherited paleotopography of the base of the Cambrian

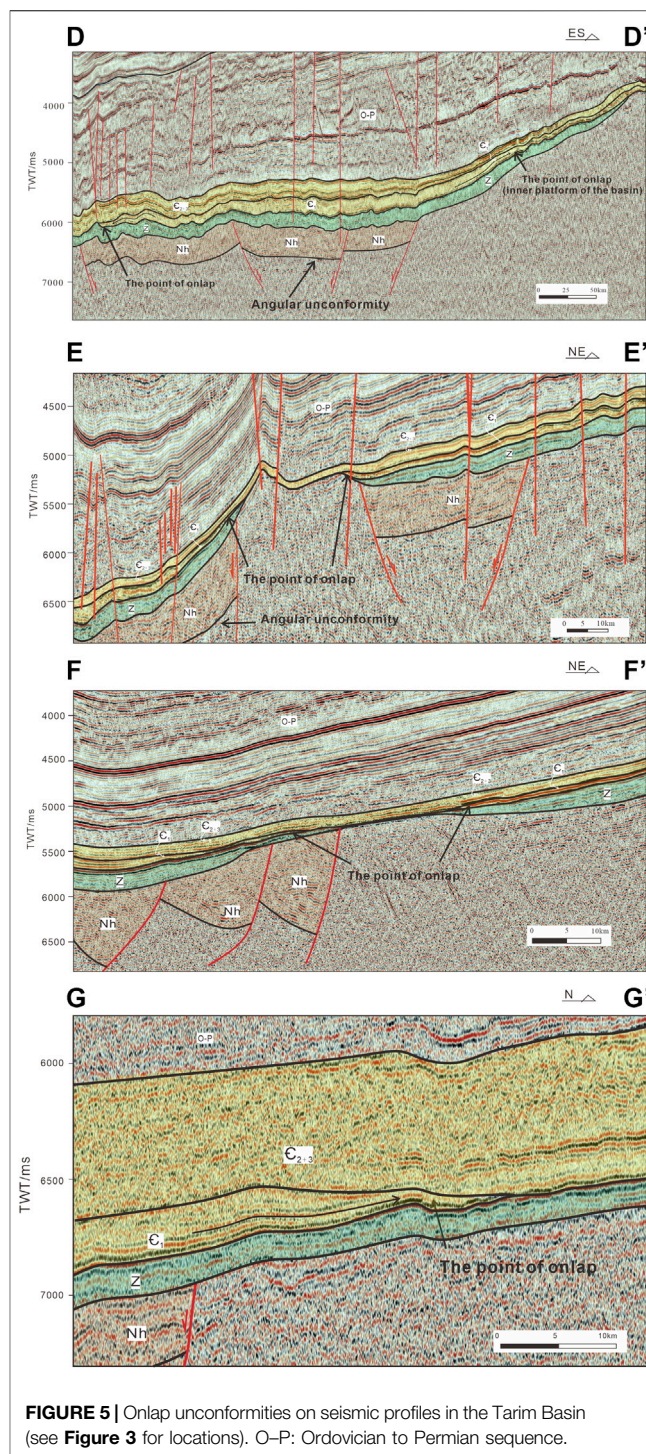


**FIGURE 5** | Onlap unconformities on seismic profiles in the Tarim Basin (see **Figure 3** for locations). O–P: Ordovician to Permian sequence.

intervals: onlap (unconformities), angular unconformities, and disconformities.

In most areas of the Tarim Basin, lower Cambrian siliceous shales overlie Sinian dolomites (**Figure 3**). Using the seismic reflection characteristics of the Nanhua–Cambrian Formations, onlaps were identified in the seismic profiles (**Figure 5**). These seismic reflections show the lower Cambrian sequences onlapping

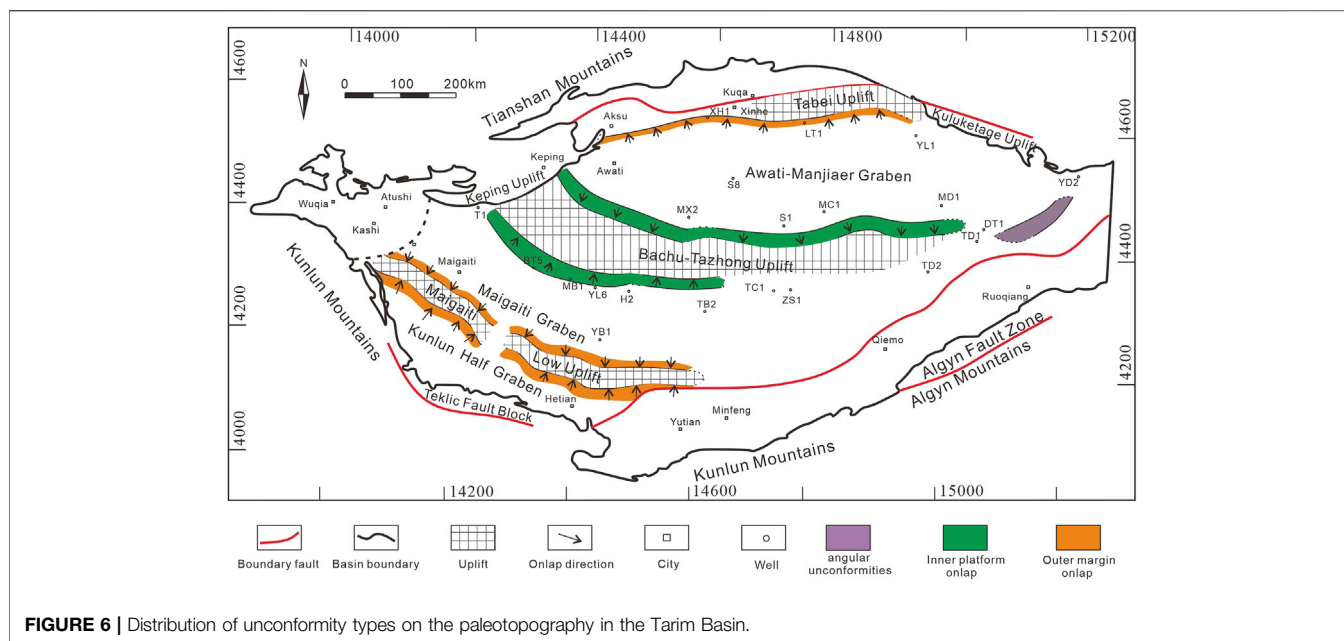


**FIGURE 6** | Distribution of unconformity types on the paleotopography in the Tarim Basin.

the paleotopography on the Precambrian basement along profiles E-E', F-F', and G-G' (Figure 5). This phenomenon illustrates that the younger sediments are progressively overstepping onto the older strata. The Qigebulak Formation dolomite rocks were onlapped by the lower Cambrian mudrocks, which were in turn onlapped by the lower-middle Cambrian dolomites. Onlap is most prominently developed in two areas, the inner platform of the basin and the basin margin (Figures 5E,F). The onlap is typically characterized by the gradual overstepping of younger sediments on each other along the paleoslope. The onlap of the inner platform mainly appears on the substratum of the lower Cambrian, and it occurs primarily along both sides of the Bachu and Tazhong uplifts. The onlap of the margin of the basin mainly appears on the lower Cambrian. It occurs along the northern and southwestern margins of the basin (Figure 6).

Progradational reflection geometries and onlaps are widely distributed in the Tarim Basin. The thickness of the lower Cambrian strata increases from the point of the onlap toward the northwest on the right side of the profile D-D' (Figure 5D), which is a characteristic of the onlap on the inner platform. The outer margin of the basin is identified on the NE-SW-trending profile E-E', which runs nearly parallel to the seismic profile F-F' and across the largest sag in the basin. The depositional extent of sedimentation in the Sinian sequences is greater than that in the Nanhua sequences, and the lower parts of the Cambrian strata gradually thicken from the point of onlap to the center of the graben (profile E-E'; Figure 5E). In the northern part of the basin, the progradational reflections in the lower part of the Cambrian strata (profile G-G'; Figure 5G) can be seen to gradually thicken from the point of onlap toward the southern Tarim Basin.

Paleo-uplifts are observed between the grabens and half-grabens of the Nanhua interval (profile E-E'; Figure 5E). The shapes of some paleo-uplifts indicate that they continued into the Cambrian strata. Three major paleo-uplifts (referred to as the Tabei Uplift, Bachu-

Tazhong Uplift, and Maigaiti Low Uplift) are observed in the Cambrian strata in the Tarim Basin (Figure 6), and all of them played an important role in the sedimentary and tectonic evolution of the Cambrian interval. The occurrence of the onlap was found on the slope paleotopography of the paleo-uplift. And the outer margin onlap occurs primarily along both sides of the Maigaiti Low Uplift and the southern part of the Tabei Uplift (Figure 6). Along both sides of the Maigaiti Uplift, the onlap unconformities are NW-SE-trending, while they trend more easterly in the eastern part. The maximum distance between the onlap points is about 100 km, and the minimum distance is about 70 km; the paleo-uplift lies between these points. Along the Tabei Uplift, the onlap unconformity is E-W trending, and the northern onlap point marks the northern ancient margin of the Tarim Basin (Figure 6). Moreover, the inner onlap unconformity connects with the ancient platform. Based on these observations, the Bachu and Tazhong uplifts formed the ancient platform during the Sinian interval. The onlap onto the inner platform occurs primarily along both sides of the Bachu and Tazhong uplifts, both of which are E-W-trending. The middle part of the inner platform onlap includes the Bachu Uplift, Tazhong Uplift, and Awati Depression at present. The onlap unconformity shows two nearly E-W-trending grabens and an inner basin platform on the paleotopography.

Angular unconformities can be seen along the SW-NE-trending seismic profile H-H' (Figure 7) along the southeastern margin of the Tarim Basin (Figure 6). This phenomenon is related to thermal subsidence, which limited exposure and erosion along the margin of the Tarim Plate and led to a high contact angle on the base of the Cambrian strata on the seismic profile, resulting in the formation of "tilting-truncating" unconformities. However, in most of the basin, especially the interior regions of the Tarim Plate, the Cambrian strata are generally conformable with the Sinian and Nanhua strata.

The Sinian Sugaitebulak Formation and the Aksu Group are angularly unconformable in the Aksu area (Figure 8A). Lower Cambrian reflectors in the basin (e.g., Figures 4,5, and 7)

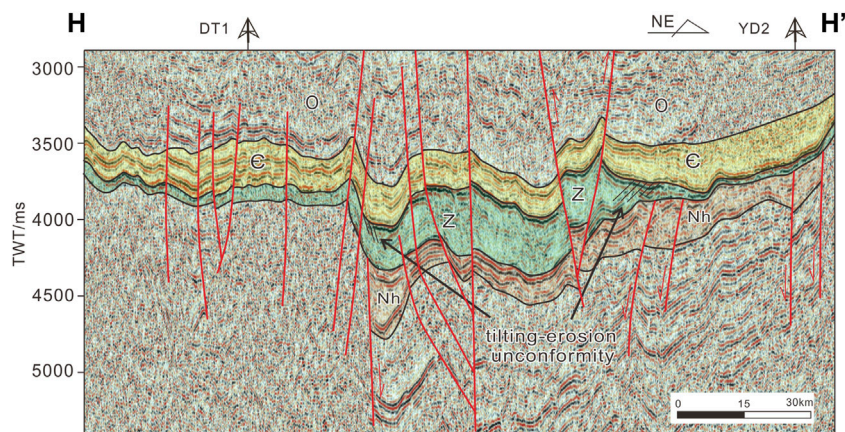


**FIGURE 7** | Interpreted seismic profile of the angular unconformity (see **Figure 3** for locations).

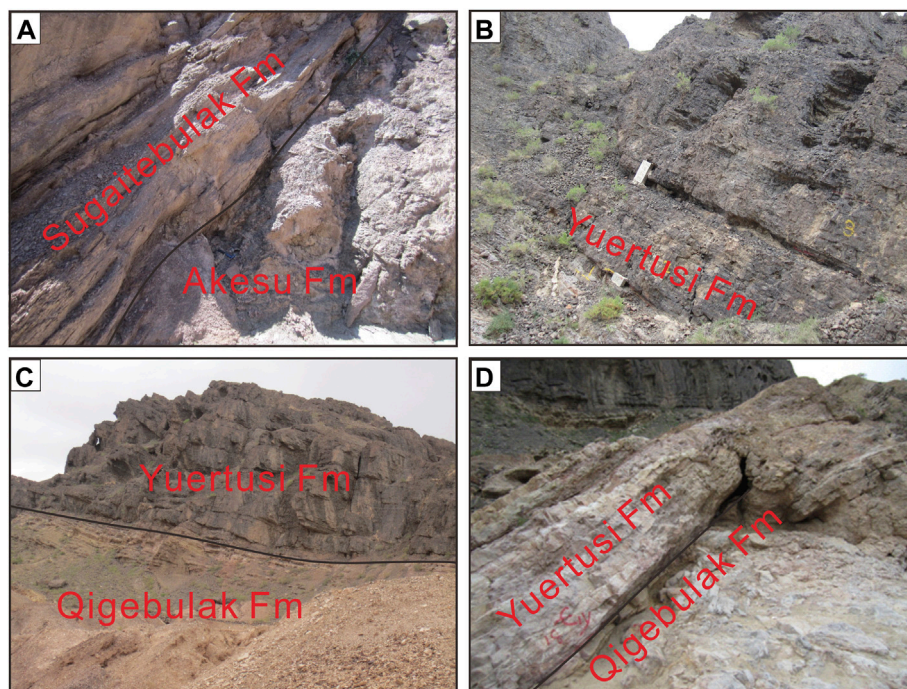


**FIGURE 8** | Field photographs of the Sinian–Cambrian boundary (the SCB) in the Aksu region (**Figure 3** for locations). (A) Aksu and Sugaitebulak formations; (B) Yuertusi Formation; (C) Yuertusi and Qigebulak formations; (D) Yuertusi and Qigebulak formations.

generally appear to be widely distributed and possess good continuity. Seismic data and field observations show that the contacts between Cambrian strata and the dolomites of the Sinian strata appear to be disconformities in many places (**Figure 8**). The outcrops of paleo-weathering crusts at the northwestern margin of the Tarim Basin in the Aksu area (He et al., 2010a; Shang et al., 2020; **Figures 8B,C**) indicate the sub-aerial exposure of the upper surfaces of the exposed Sinian sediments in the Aksu region. Other indicators include mud cracks, color, and lithology changes at the SCB (**Figure 8C**), karst breccias, dolomites, and thin soil layers with weathered crusts

(**Figure 8D**). Weathered crusts are also observed between the Cambrian and Sinian sequences in the Kuruktag area (Shang et al., 2020). Such weathered crusts are closely related to the process of angular unconformities forming.

### Sedimentary Thicknesses of the Nanhua and Sinian Successions

The distribution of the Sinian interval and lower Cambrian strata appears to be correlated with the range of distribution of

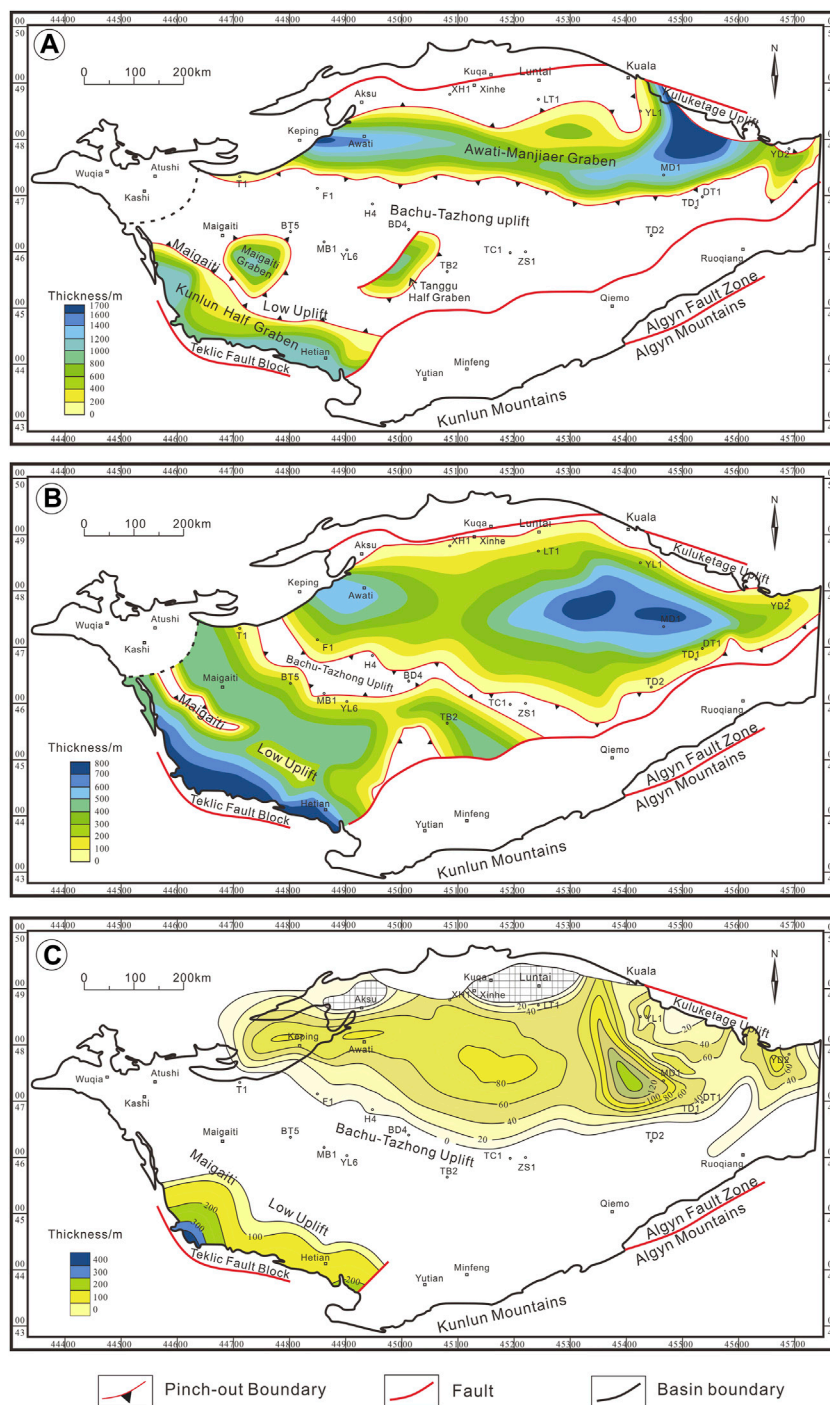


**FIGURE 9** | Isopachs of the strata in the Tarim Basin. **(A)** Thickness variations within the Nanhua interval; **(B)** Thickness variations within the Sinian interval; **(C)** Thickness variations within the Yuertusi Formation of the Lower Cambrian.

different types of unconformities (Figures 6,9). The Nanhua–Sinian depositional sequence appears to behave as a typical rift-to-post-rift (thermal subsidence) succession. The rift basin in the Nanhua sequence contains two sub-basins. The first is the Awati-Manjiaer Graben, whose depocenter is defined by an approximately E–W trending, 600–800 km, long ribbon-

shaped, sub-basin developed within the Nanhua graben in the northern Tarim Basin, while a second depocenter occurs in the Kunlun Half-Graben in the south (Figure 9A). In addition, the Maigaiti Graben and Tanggu Half-Graben occur as a ca.350 m thick sequence in a sub-elliptical and rhombic depocenter. The isopach map of the Sinian sequence also

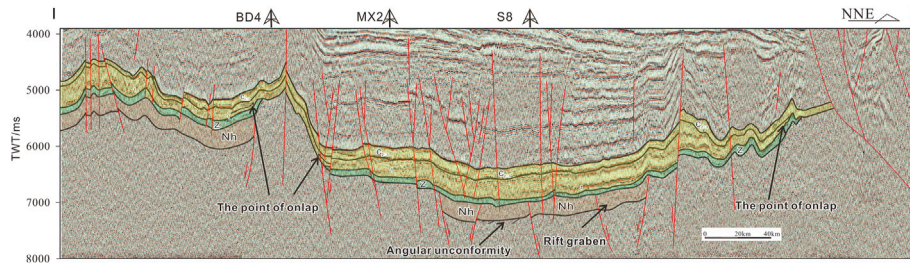


**FIGURE 10** | Seismic profile across the Tarim Basin showing the structural framework (Figure 3 for locations).

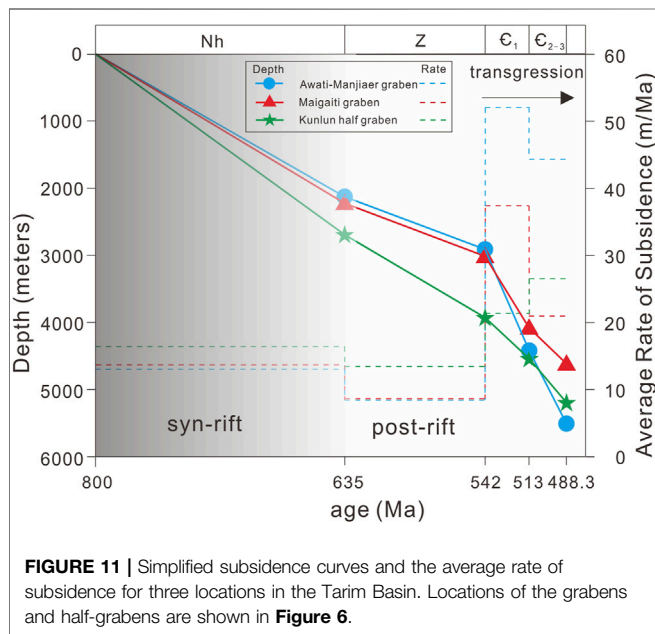


**FIGURE 11** | Simplified subsidence curves and the average rate of subsidence for three locations in the Tarim Basin. Locations of the grabens and half-grabens are shown in Figure 6.

suggests the occurrence of two sub-basins (Figure 9B). The Awati–Manjiaer Graben contains a ca.650 m interval of Sinian sediments in an approximately E–W trending depocenter, which is similar to the structures observed in the isopach map of the Nanhua sequence (Figure 9A). The maximum thickness in this area reaches ca.1,600 m in the southwest part of the Kuluketage Uplift. The second sub-basin is the Kunlun Half-Graben, which is defined by the NW–SE trending, 300–400 km long, ribbon-shaped depocenter developed along the Teklic fault block.

The depositional extent of the Sinian is greater than that of the Nanhua succession and gradually decreases from west to east (Figure 9B). The NW–SE-trending Maigaiti Low Uplift is located between the Kunlun Half-Graben and the Maigaiti Graben (at the location of the marginal fault to the north of the Kunlun Half-Graben in Figure 9A), where Sinian strata were not deposited. More importantly, the sedimentary thickness of the Lower Cambrian Yuertusi Formation gradually decreases along the Teklic fault block to the north (Figure 9C), which indicates that the Maigaiti Low Uplift also occurs in the Lower Cambrian interval in the southern Tarim Basin. This is

consistent with the distribution of onlap unconformities (Figure 6). As for the interior of the Tarim Basin, the NW–SE trend of the Bachu–Tazhong Uplift continues into the Early Cambrian (Figures 9B,C). Seismic profiles (Figure 5) show that the onlap unconformity of the Lower Cambrian sediments covers the Sinian strata along the margin of the Maigaiti Low Uplift and the Bachu–Tazhong Uplift. These structures and the stratigraphic thicknesses suggest that sedimentation occurred over an expanded area after the Nanhua continental rifting. Widespread deposition of post-rift Sinian sediments occurred in this area and caused the burial of the Nanhua grabens or half-grabens. As previously stated, the Maigaiti Low Uplift and Bachu–Tazhong Uplift strongly controlled the sedimentary distribution and the migration of the depocenter in the Tarim Basin during the Nanhua–Early Cambrian intervals.

## DISCUSSION

### Tectonic Evolution of the Sinian-Cambrian Successions and the Inherited Paleotopography

Based on the aforementioned study, the Nanhua sequence is a rift basin. Seismic profiles demonstrate that the structure and sedimentation in the Nanhua system were controlled primarily by normal faults (Figures 5,10). And the rift period was characterized by rapid tectonic subsidence and the infilling of large amounts of sediments (e.g., Allen and Allen, 2013) (Figure 10). The overlying Sinian sequence is a post-rift basin, and the lateral extent of Sinian deposition over the Nanhua sedimentary sequences has increased (Figure 10). Moreover, the similarities between the relative thicknesses of the Cambrian and Sinian strata suggest that the paleotopography of the Cambrian was similar to that of the underlying Sinian sediment. The similarity of stratum thickness indicates that the paleotopography on the Precambrian basement inherited the surface morphology after the active tectonic subsidence during the rifting period.

The initial continental rifting of the Rodinia supercontinent is thought to have occurred at ca. 800 Ma (Xu et al., 2005; Tang et al., 2006; Lu et al., 2008; Zhang et al., 2009; Xu et al., 2011; Tang et al., 2016), and to have led to the sedimentation of the

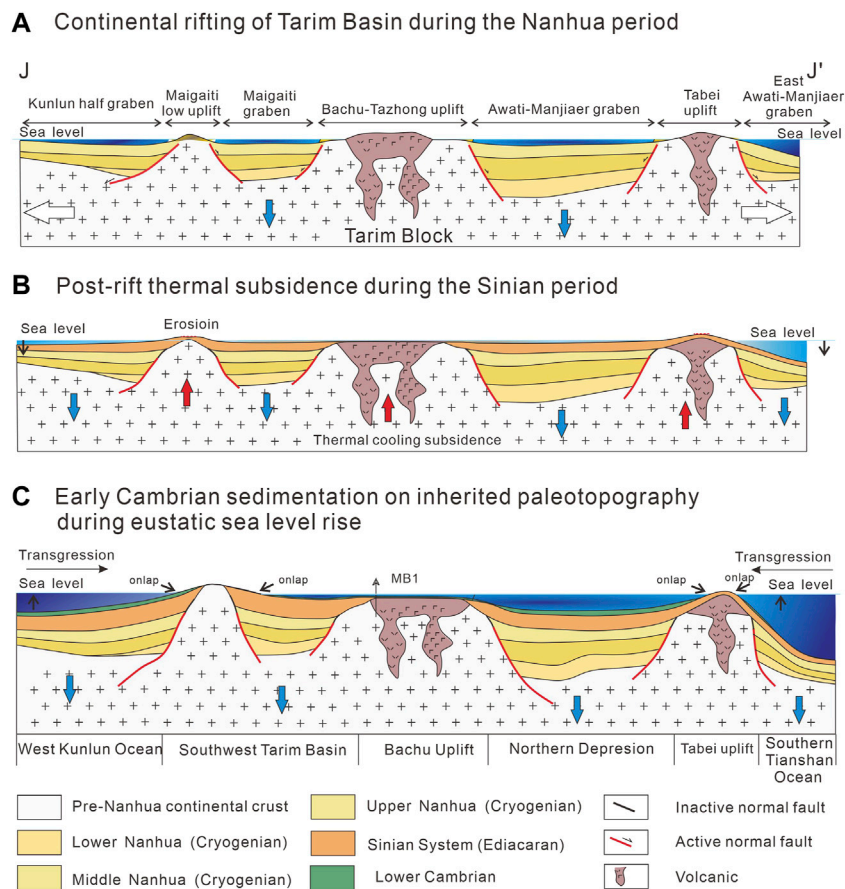


**FIGURE 12 |** Sequential tectonic diagrams depicting the geological evolution of the Tarim Basin (**Figure 3** for locations).

Nanhua sequence. The occurrences of the continental rifting events are consistent with the ages of the volcanic rocks ( $722 \pm 3$  Ma; Wu et al., 2012), which are intercalated with coeval sedimentary rock units in the Tarim Basin (Xu et al., 2009; Wang et al., 2010; Xu et al., 2013; Ren et al., 2018; Zhang et al., 2019). There was one rift system including two rift axes in the Tarim Basin during the Nanhua period, the Awati–Manjiaer Graben, and the Kunlun Half-Graben (**Figure 9A**). In seismic profiles, the Nanhua sequence demonstrates an angular unconformable relation with the pre-Neoproterozoic basement (Wu et al., 2016; Ren et al., 2018; **Figures 5, 10**). The two rift axes in the Nanhua period are fault-controlled; they are characterized by the accumulation of magmatic and clastic rocks and multi-episodic magmatism. This multi-episodic magmatism is consistent with the multi-phase rifting at 740–760 Ma, 660–681 Ma, and 635–650 Ma (Xu et al., 2005; Lu et al., 2008; Zhang et al., 2009). Zhu et al. (2008) and Wen et al. (2017) identified a rifting extension in the northern Kuruktag area occurring from ca. 650 to 630 Ma. These tectonic movements resulted in extensive rifting in the Tarim Basin during the early Nanhua period, which led to the development of the rift grabens in the Nanhua strata (**Figure 10**).

After intense extension and rapid subsidence during the rifting stage, the basin entered the post-rifting stage, i.e., the thermal subsidence stage (**Figure 11**). Compared with the tectonic subsidence during the rifting, the most important feature of the thermal subsidence is the slow subsidence rate (**Figure 11**). The thermal subsidence is generally fairly long-lived (Jarvis and McKenzie, 1980; Meng et al., 2011). And this thermal subsidence lasted the whole Sinian in the Tarim Basin. With the exception of wells MB1-YL6-TC1-ZS1 on the Tazhong Uplift, most wells in the Tarim Basin penetrated at least some Sinian sediments (**Figure 3**), which shows that the Sinian sediments were deposited over a wide area. The broad geographic extent of the deposition can also be observed in the seismic profiles (**Figures 5,7,10**). This increase in the geographic extent of Sinian deposition due to extensive thermal subsidence is a principal feature of sedimentation during the Sinian (**Figure 12B**). The average rates of subsidence for the Awati–Manjiaer Graben and Maigaiti Graben are similar (12.9 and 13.5 m/my, respectively). The Kunlun Half-Graben, which has a higher subsidence rate (16.31 m/my), is located at the margin of the Tarim block. The subsidence rates for the Awati–Manjiaer Graben and Maigaiti Graben during the Sinian are nearly half

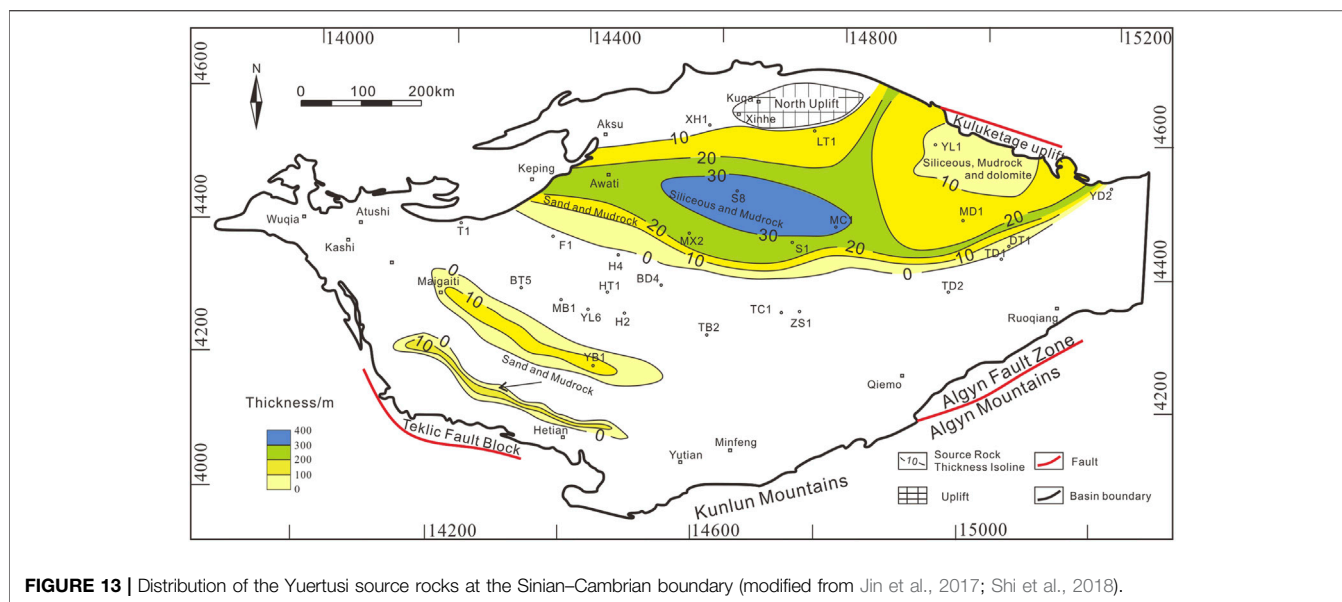


**FIGURE 13** | Distribution of the Yuertusi source rocks at the Sinian–Cambrian boundary (modified from Jin et al., 2017; Shi et al., 2018).

those during the Nanhua period (8.4 and 8.0 m/my, respectively). During this thermal subsidence process, the original paleo-uplift morphology was retained, and the Sinian strata were eroded there (Figures 5,12). The distribution of angular unconformities mainly along the southeastern margin of the Tarim Basin illustrated that the thermal subsidence was the dominant phenomenon, and it caused the down-warping of the lithosphere and affected much broader areas (e.g., Royden and Dövényi, 1988; Corver et al., 2009).

Since the Early Cambrian, carbonate rocks grew rapidly upward owing to the rapid transgression and sufficient sediment supply (e.g. Wolstencroft et al., 2014; He et al., 2017). A major transgression caused by rapid subsidence of the Tarim Basin took place during the Cambrian, which gave rise to extensive shallow epicontinental seas defined as platforms (Figure 6). And the Awati–Manjiaer Graben had the highest subsidence rate of 51.97 m/my (Figure 11).

The Tarim Basin was located on a stable craton during the late Sinian to the Early Cambrian, and it is characterized by stable sedimentary structures (Meert and Van Der Voo, 1997; Kröner and Stern, 2005; Zhang et al., 2019). Consequently, the strata thickness distribution maps of the Nanhua–Cambrian sequences (Figures 9A,B) are very consistent and show that the depocenters and sedimentation patterns of the Sinian and Nanhua sequences are closely related. And the Tarim Basin did not experience a change in its tectonic and sedimentary frameworks during this period. The Bachu–Tazhong Uplift was denuded, after which sedimentation occurred on the platform due to the relative sea level rise. The seismic profiles (Figure 5) indicate that the paleotopography of the early Cambrian was inherited from the late Sinian, after which the strata underwent rapid subsidence during the early Cambrian

(Figure 12C). In addition, the lower Cambrian strata thickened from the onlap point in the direction of the inner graben (Figure 5).

## Relations of Onlap and Yuertusi Source Rock

It was found that the total organic carbon (TOC) of marine argillaceous source rocks could be high, and Yuertusi source rock also have similar characteristics (Zhu et al., 2016; Cui et al., 2017). We found that the TOC content of Yuertusi source rocks on the intra-platform slope is high. For example, the TOC values of the Yuertusi source rocks are in the range of 2–16% in the Aksu outcrops; in the Shaiirike outcrops, TOC values can be as high as 4–16% (He et al., 2010b; Zhu et al., 2016). TOC values of the samples from Well XH1, LT-1, and TS-1 were in the range of 4–16% (Wu et al., 2016; Zhu et al., 2016; Yang et al., 2020). In addition, the black shale of the Yuertusi source rock was formed in a weakly alkaline environment during a widespread transgression (Wu et al., 2021). The intra-platform slope is an ideal place for shale deposition (Ngozi, 2017). So, the high TOC values of the Yuertusi source rock is related to the intra-platform slope in a relatively shallow marine environment (Ofuebe, 2015).

The time of rapid subsidence in the Tarim Basin corresponds to the highest paleoheat flow and the rapid rise of paleogeotemperature during the Cambrian (He et al., 2017). The significant increases in the thickness of the mudstones and siltstones in the lower Cambrian in the vicinity of Well XH1 in the northern part of the basin indicate that the water depth was increasing at this time (Shi et al., 2017; Wen et al., 2017; Figure 4). During this period, the widespread transgressions formed the continental deposits along the slope of the paleotopography. And the sediment onlap patterns were recorded by the onlap unconformities (Figures 6,9C). The organic-rich

mudstones and siliceous rocks of the Yuertusi Formation were deposited in the inner Tarim Basin and at the southwestern margin of the Tarim Basin as a result of the transgressive events associated with tectonic stability, gentle slope, and post-glacial sea level rise (Figure 12C). The basin was tectonically stable during these transgressional events; this stability lasted until at least the early Ordovician (He et al., 2007; Zhao et al., 2011; Zhang et al., 2019), during which time extensive marine carbonates were deposited.

The bottom of the Cambrian Formation in wells YL1 and XH1 (Figure 4), located in the southern portion of the onlap unconformity, is mainly composed of siliceous rocks and shales. The petrological characteristics of the rocks indicate that the Yuertusi shales were deposited on a gently sloping carbonate platform with coastal upwelling (Zhao et al., 2011; Zhu et al., 2016; Zhu et al., 2018; Zhang et al., 2020). Transgression is represented by the increase in the water depth at a constant rate, and in this case, the Tarim Basin margin is maintained as two segments, a horizontal shelf with eustatic fluctuations and a gentle slope with a fixed angle (e.g., Christie-Blick, 1991; Figure 9). Under the transgressive system during the Early Cambrian, the position of the onlap unconformity is marked by the zone of transition between the gentle slope of the Awati–Manjiaer Graben and the Tabei Uplift (Figure 6). This suggests that the gentle slope of the Awati–Manjiaer Graben in the southern part of the onlap unconformity is conducive to the deposition of shales, which can be high-quality source rocks (Figure 13). In the central uplift, the Yuertusi Formation is absent in wells BT5-MB1-TC1-ZS1 (Figure 3). When combined with the stratigraphic framework, it appears that inherited paleotopography controlled the distribution of the Yuertusi source rocks. Yuertusi source rocks in the southwestern part of the basin will be located in the southwest onlap unconformity (Figures 6,13), while the W–E margin of the southern uplift is consistent with the inner platform onlap unconformity zone. In summary, the gentle slope of the fixed-gradient region is conducive to the deposition of shales, which are good source rocks with a suitable deep-water environment and stable sediment supply. The Yuertusi source rocks are interpreted to onlap the inner platform of the inherited paleotopography. And we accurately determined the distribution range of the Yuertusi source rocks in the Awati–Manjiaer Graben according to the distribution range of onlap on the paleotopography (Figure 13).

## CONCLUSION

- 1) There was a one rift system including two rift axes in the Tarim Basin during the Nanhua period, the Awati–Manjiaer

## REFERENCES

- Allen, P. A., and Allen, J. R. (2013). *Basin Analysis: Principles and Application to Petroleum Play Assessment*. Hoboken, New Jersey: John Wiley & Sons, 45–60.
- Cai, X. Y. (2007). Main Factors Controlling Hydrocarbon Accumulation of Middle-And Large-Sized Oil and Gas Fields and Their Distribution Rules in

Graben, and the Kunlun Half-Graben. The extensive thermal subsidence lasted the whole Sinian period, and makes the paleotopography on the Precambrian basement inherited the landform after the Nanhua continental rifting.

- 2) The source rock deposits forming the inner platform onlap and outer margin onlap on the inherited paleotopography. And the onlap reflects the distribution range of the Yuertusi source rocks in the Cambrian.
- 3) A major transgression caused by the rapid subsidence of the Tarim Basin took place during the Cambrian, which has formed the Yuertusi source rocks on the inherited paleotopography.

## DATA AVAILABILITY STATEMENT

The original contributions presented in the study are included in the article/Supplementary Material, further inquiries can be directed to the corresponding author.

## AUTHOR CONTRIBUTIONS

HY and SC presented the idea and design of the research. HY and SC wrote the article and led the data analysis and interpreted the results with KD, XG, LK, NF, HZ, and WY. All.

## FUNDING

This work was financially supported by the National Key Research and Development Program of China (No.2017YFC0603105), National Natural Sciences Foundation of China (Grant No: 42172138) and The Strategic Priority Research Program of the Chinese Academy of Sciences (Grant No: XDA14010306).

## ACKNOWLEDGMENTS

We thank the Editor, S. Jiang, and reviewers for their constructive comments.

## SUPPLEMENTARY MATERIAL

The Supplementary Material for this article can be found online at: <https://www.frontiersin.org/articles/10.3389/feart.2022.864082/full#supplementary-material>

the Tarim Basin. *Oil Gas Geol.* 28 (6), 693–1702. doi:10.3321/j.issn:0253-9985.2007.06.001

Christie-Blick, N. (1991). Onlap, Offlap, and the Origin of Unconformity-Bounded Depositional Sequences. *Mar. Geol.* 97 (1), 35–56. doi:10.1016/0025-3227(91)90018-Y

Corver, M. P., Doust, H., van Wees, J. D., Bada, G., and Cloetingh, S. (2009). Classification of Rifted Sedimentary Basins of the Pannonian Basin System

- According to the Structural Genesis, Evolutionary History and Hydrocarbon Maturation Zones. *Mar. Petroleum Geol.* 26 (8), 1452–1464. doi:10.1016/j.marpetgeo.2008.12.001
- Cui, H., Tian, L., Liu, J., and Zhang, N. (2017). Hydrocarbon Discovery in the Ordovician Dolomite Reservoirs in the Maigaiti Slope, Southwest Depression of the Tarim Basin, and its Exploration Implications. *Nat. Gas. Ind. B* 4 (5), 354–363. doi:10.1016/j.ngib.2017.09.005
- Feng, X. K., Liu, Y. B., Han, C. W., Yan, W., Dong, L., and He, Y. F. (2015). Sinian Rift Valley Development Characteristics in Tarim Basin and its Guidance on Hydrocarbon Exploration. *Petroleum Geol. Eng.* 29 (2), 5–10. doi:10.1016/j.ptlrs.2017.04.004
- Ge, R., Zhu, W., and Wilde, S. A. (2016). Mid-Neoproterozoic (Ca. 830–800 Ma) metamorphicP-Tpaths Link Tarim to the Circum-Rodinia Subduction-Acretion System. *Tectonics* 35 (6), 1465–1488. doi:10.1002/2016tc004177
- Guo, Z. J., Zhang, Z. C., Liu, S. W., and Li, H. M. (2003). U–pb Geochronological Evidence for the Early Precambrian Complex of the Tarim Craton, NW China. *Acta Petrol. Sin.* 19 (3), 537–542. doi:10.3321/j.issn:1000-0569.2003.03.020
- Han, Q., Zhu, Y. H., Zhu, C. L., Wang, C., Chen, Z. L., and Fei, J. W. (2016). Petrological Characteristics and Zircon U–Pb Age for Magmatic Rocks from Pre-sinian Basement of the SDQ Area of Shaya Rise in Tarim Basin, NW China. *Acta Petrol. Sin.* 32, 1493–1504 (in Chinese with English abstract).
- He, B., Jiao, C., Xu, Z., Cai, Z., Zhang, J., Liu, S., et al. (2016). The Paleotectonic and Paleogeography Reconstructions of the Tarim Basin and its Adjacent Areas (NW China) during the Late Early and Middle Paleozoic. *Gondwana Res.* 30, 191–206. doi:10.1016/j.gr.2015.09.011
- He, D. F., Bai, W. M., and Meng, Q. R. (1998). Geodynamic Evolution and Petroliferous System Cycle in Tarim Basin. *Acta Geophys. Sin.* 41 (2), 77–87. (in Chinese with English abstract).
- He, D. F., Zhou, X. Y., Zhang, C. J., Yang, W. J., and Shi, X. (2006). Characteristics of Geologic Framework of Multicycle Superimposed Basin in Tarim Basin. *China Pet. Explor.* 11 (1), 31–41. doi:10.3969/j.issn.1672-7703.2006.01.006 (in Chinese with English abstract)
- He, D. F., Zhou, X. Y., Zhang, C. J., and Yang, X. F. (2007). Tectonic Types and Evolution of Ordovician Proto-type Basins in the Tarim Region. *Chin. Sci. Bull.* 52 (1), 164–177. doi:10.1007/s11434-007-6010-z
- He, F., Lin, C. S., Liu, J. Y., Zhang, Z. L., Zhang, J. L., Yan, B., et al. (2017). Migration of the Cambrian and Middle-Lower Ordovician Carbonate Platform Margin and its Relation to Relative Sea Level Changes in Southeastern. *Tarim Basin Oil Gas Geol.* 38 (4), 711–721. doi:10.11743/ogg20170408
- He, J. Y., Jia, C. Z., Wu, G. H., and Xu, B. (2010a). Characteristics and Model of Sinian Weathering Paleo-Karst in Aksu Area, Xinjiang. *Acta Petrol. Sin.* 26 (8), 2513–2518. doi:10.3724/SP.J.1084.2010.00199
- He, J. Y., Wu, G. H., Xu, B., Qu, T. L., Li, H. H., and Cao, Y. H. (2010b). Characteristics and Petroleum Exploration Significance of Conformity between Sinian and Cambrian in Tarim Basin. *Chin. J. Geol.* 45 (3), 698–706. doi:10.3969/j.issn.0563-5020.2010.03.006 (in Chinese with English abstract)
- Jarvis, G. T., and McKenzie, D. P. (1980). Sedimentary Basin Formation with Finite Extension Rates. *Earth Planet. Sci. Lett.* 48 (1), 42–52. doi:10.1016/0012-821x(80)90168-5
- Jia, C. Z. (1997). *Tectonic Characteristics and Petroleum Deposits of Tarim Basin in China*. Beijing: Petroleum Industry Press.
- Jiang, L., Cai, C., Worden, R. H., Crowley, S. F., Jia, L., Zhang, K., et al. (2016). Multiphase Dolomitization of Deeply Buried Cambrian Petroleum Reservoirs, Tarim Basin, North-West China. *Sedimentology* 63 (7), 2130–2157. doi:10.1111/sed.12300
- Jin, Z., Liu, Q. Y., Liu, Q., and Yun, J. (2017). Potential Petroleum Sources and Exploration Directions Around the Manjar Sag in the Tarim Basin. *Sci. China Earth Sci.* 60 (2), 235–245. doi:10.1007/s11430-015-5573-7
- Jin, Z., and Wang, Q. C. (2004). Recent Developments in Study of the Typical Superimposed Basins and Petroleum Accumulation in China: Exemplified by the Tarim Basin. *Sci. China Ser. D.* 47 (14), 1. doi:10.1360/04zd0020
- Kröner, A., and Stern, R. (2005). “AFRICA| Pan-African Orogeny,” in *Encyclopedia of Geology*. Editors R.C. eSelle, L.R.M. Cocks, and I.R. Plimer (Oxford: Elsevier).
- Li, W. X., Li, X. H., and Li, Z. X. (2010). Ca. 850 Ma Bimodal Volcanic Rocks in Northeastern Jiangxi Province, South China: Initial Extension during the Breakup of Rodinia? *Am. J. Sci.* 310 (9), 951–980. doi:10.2475/09.2010.08
- Lu, S. N., Li, H. K., Zhang, C. L., and Niu, G. H. (2008). Geological and Geochronological Evidence for the Precambrian Evolution of the Tarim Craton and Surrounding Continental Fragments. *Precambrian Res.* 160 (1–2), 94–107. doi:10.1016/j.precamres.2007.04.025
- Lu, X., Wang, Y., Yang, D., and Wang, X. (2020). Characterization of Paleo-Karst Reservoir and Faulted Karst Reservoir in Tahe Oilfield, Tarim Basin, Chinafield, Tarim Basin, China. *Adv. Geo-Energy Res.* 4 (3), 339–348. doi:10.46690/ager.2020.03.11
- Luo, C., Liu, S. G., Sun, W., Ran, B., Yong, Z., Yang, D., et al. (2014). Basic Characteristics of Shale Gas in the Lower Cambrian Niutitang Formation in the Upper Yangtze Region: Taking Nangao Section in Danzhai as an Example. *Nat. Gas. Geosci.* 25 (3), 453–460. doi:10.11764/j.issn.1672-1926.2014.03.0453
- Luo, Z. L. (1998). Distribution and Outlook for Oil/gas Exploration of Petroliferous Basin in China. *Xinjiang Pet. Geol.* 19, 441–449. (in Chinese with English abstract).
- McKenzie, D. (1978). Some Remarks on the Development of Sedimentary Basins. *Earth Planet. Sci. Lett.* 40 (1), 25–32. doi:10.1016/0012-821x(78)90071-7
- Meert, J. G., and Van Der Voo, R. (1997). The Assembly of Gondwana 800–550 Ma. *J. Geodyn.* 23 (3), 223–236. doi:10.1016/s0264-3707(96)00046-4
- Meng, Q.-R., Wei, H.-H., Qu, Y.-Q., and Ma, S.-X. (2011). Stratigraphic and Sedimentary Records of the Rift to Drift Evolution of the Northern North China Craton at the Paleo- to Mesoproterozoic Transition. *Gondwana Res.* 20 (1), 205–218. doi:10.1016/j.gr.2010.12.010
- Ofuebe, N. (2015). *Source Rock Evaluation and Depositional Environment of Middle Eocene–Early Miocene Sediments in Umuahia and it’S Eviron. Niger Delta Basin, Southeastern Nigeria*.
- Ren, J. S., Wang, Z. X., and Chen, B. W. (1999). *Analysis of Tectonic Structure in China from a Worldwide Point of View—A Brief Description of Tectonic Structure Maps of China and its Adjacent Areas*. Beijing: Geologic Publishing House.
- Ren, R., Guan, S., Wu, L., and Zhu, G. (2018). Evolution of the Neoproterozoic Rift Basins and its Implication for Oil and Gas Exploration in the Tarim Basin. *Petroleum Res.* 3 (1), 66–76. doi:10.1016/j.ptlrs.2018.03.003
- Royden, L., and Dövényi, P. (1988). “Variations in Extensional Styles at Depth across the Pannonian Basin System: Chapter 17,”. Editors L.H. Royden and F. Horva’t (American Association of Petroleum Geologists, Memoirs), 45, 235–255. *Pannonian Basin a Case Study Basin Evol.*
- Shang, Y., Gao, Z., Fan, T., Wei, D., Wang, Z., and Karubandika, G. M. (2020). The Ediacaran-Cambrian Boundary in the Tarim Basin, NW China: Geological Data Anomalies and Reservoir Implication. *Mar. Petroleum Geol.* 111, 557–575. doi:10.1016/j.marpetgeo.2019.08.032
- Shi, K. B., Liu, B., Tian, J. C., and Pan, W. Q. (2016). Sedimentary Characteristics and Lithofacies Paleogeography of Sinian in Tarim Basin. *Acta Pet. Sin.* 37 (11), 1343–1360. doi:10.7623/syxb201611003
- Shi, K., Liu, B., Jiang, W., Gao, X., Liu, S., and Shen, Y. (2017). Sedimentary and Evolutionary Characteristics of Sinian in the Tarim Basin. *Petroleum Res.* 2 (3), 264–280. doi:10.1016/j.ptlrs.2017.04.004
- Shi, K., Liu, B., Jiang, W., Luo, Q., and Gao, X. (2018). Nanhua-Sinian Tectono-Sedimentary Framework of Tarim Basin, NW China. *Oil Gas Geol.* 39 (5), 862–877. doi:10.11743/ogg20180502
- Tang, L. J., Lü, X. X., Jin, Z. J., Liu, X. P., and Qiu, N. S. (2006). Petroleum Geological Characteristics, Strategic Exploration Area Selection and Urgent Geological Problems of Marine Carbonate Sequences in China. *Geol. Bull. China* 25 (9–10), 1032–1035. doi:10.1177/001872086300500510
- Tang, Q., Zhang, Z., Li, C., Wang, Y., and Ripley, E. M. (2016). Neoproterozoic Subduction-Related Basaltic Magmatism in the Northern Margin of the Tarim Craton: Implications for Rodinia Reconstruction. *Precambrian Res.* 286, 370–378. doi:10.1016/j.precamres.2016.10.012
- Turner, S. A. (2010). Sedimentary Record of Late Neoproterozoic Rifting in the NW Tarim Basin1-4. *China Precambrian Res.* 181, 85–96. doi:10.1016/j.precamres.2010.05.015
- Veeken, P. C. (2006). *Seismic Stratigraphy, Basin Analysis and Reservoir Characterisation*. Amsterdam, Netherlands: Elsevier.
- Wang, F., Wang, B., and Shu, L. S. (2010). Continental Tholeiitic Basalt of the Aksu Area (NW China) and its Implication for the Neoproterozoic Rifting in the

- Northern Tarim. *Acta Petrol. Sin.* 26 (2), 547–558. doi:10.3724/SP.J.1084.2010.00199
- Wen, B., Evans, D. A. D., and Li, Y.-X. (2017). Neoproterozoic Paleogeography of the Tarim Block: An Extended or Alternative "Missing-Link" Model for Rodinia? *Earth Planet. Sci. Lett.* 458, 92–106. doi:10.1016/j.epsl.2016.10.030
- Wolstencroft, M., Shen, Z., Törnqvist, T. E., Milne, G. A., and Kulp, M. (2014). Understanding Subsidence in the Mississippi Delta Region Due to Sediment, Ice, and Ocean Loading: Insights from Geophysical Modeling. *J. Geophys. Res. Solid Earth* 119 (4), 3838–3856. doi:10.1002/2013jb010928
- Wu, G. H., Li, H. W., Xu, Y. L., Su, W., Chen, Z. Y., and Zhang, B. S. (2012). The Tectonothermal Events, Architecture and Evolution of Tarim Craton Basement Palaeo-Uplifts. *Acta Petrol. Sin.* 28 (8), 2435–2452. (in Chinese with English abstract). doi:10.1007/s10114-012-1153-5
- Wu, L., Guan, S., Ren, R., Wang, X., Yang, H., Jin, J., et al. (2016). The Characteristics of Precambrian Sedimentary Basin and the Distribution of Deep Source Rock: A Case Study of Tarim Basin in Neoproterozoic and Source Rocks in Early Cambrian, Western China. *Petroleum Explor. Dev.* 43 (6), 988–999. doi:10.1016/s1876-3804(16)30116-1
- Wu, L., Zhu, G., Yan, L., Feng, X., and Zhang, Z. (2021). Late Ediacaran to Early Cambrian Tectonic–Sedimentary Controls on Lower Cambrian Black Shales in the Tarim Basin, Northwest China. *Glob. Planet. Change* 205, 103612. doi:10.1016/j.gloplacha.2021.103612
- Xinjiang Bureau of Geology and Mineral Resources (1993). *Regional Geology of the Xinjiang Uyghur Autonomous Region*. China: Geological Publishing House, 17–45. (in Chinese).
- Xu, B., Xiao, S. H., Zou, H. B., Chen, Y., Li, Z. X., Song, B., et al. (2009). SHRIMP Zircon U–Pb Age Constraints on Neoproterozoic Qurqatagh Diamictites in NW China. *Precambrian Res.* 168 (3–4), 247–258. doi:10.1016/j.precamres.2008.10.008
- Xu, X. S., Wang, Z. J., Wan, F., and Fu, H. (2005). Tectonic Paleogeographic Evolution and Source Rocks of the Early Paleozoic in the Tarim Basin: Dixue Qianyuan. *Earth Sci. Front.* 12 (3), 49–57.
- Xu, Z.-Q., He, B.-Z., Zhang, C.-L., Zhang, J.-X., Wang, Z.-M., and Cai, Z.-H. (2013). Tectonic Framework and Crustal Evolution of the Precambrian Basement of the Tarim Block in NW China: New Geochronological Evidence from Deep Drilling Samples. *Precambrian Res.* 235, 150–162. doi:10.1016/j.precamres.2013.06.001
- Xu, Z. Q., Li, S. T., Zhang, J. X., Yang, J. S., He, B. Z., Li, H. B., et al. (2011). Paleo-Asian and Tethyan Tectonic Systems with Docking the Tarim Block. *Acta Petrol. Sin.* 27 (1), 1–22.
- Yan, W., Wu, G. H., Zhang, Y. Q., Yang, G., Luo, H., and Wang, X. M. (2018). Sinian-Cambrian Tectonic Framework in the Tarim Basin and its Influences on the Paleogeography of the Early Cambrian. *Geotect. Metallogenia* 42 (3), 455–466. (in Chinese with English abstract). doi:10.16539/j.ddgzycx.2018.03.004
- Yang, H. J., Chen, Y. Q., Tian, J., Du, J. H., Zhu, Y. F., Li, H. H., et al. (2020). Great Discovery and its Significance of Ultra-deep Oil and Gas Exploration in Well Luntan-1 of the Tarim Basin. *China Pet. Explor.* 25 (2), 62–72. (in Chinese with English abstract).
- Yu, B. S., Ruan, Z., Zhang, C., Pan, Y. L., Lin, C. S., and Wang, L. D. (2016). Tectonic Evolution of Tarim Basin in Cambrian–Ordovician and its Implication for Reservoir Development, NW China. *J. Earth Syst. Sci.* 125 (2), 285–300.
- Zhang, C.-L., Li, Z.-X., Li, X.-H., and Ye, H.-M. (2009). Neoproterozoic Mafic Dyke Swarms at the Northern Margin of the Tarim Block, NW China: Age, Geochemistry, Petrogenesis and Tectonic Implications. *J. Asian Earth Sci.* 35 (2), 167–179. doi:10.1016/j.jseas.2009.02.003
- Zhang, C.-L., Zou, H.-B., Li, H.-K., and Wang, H.-Y. (2013). Tectonic Framework and Evolution of the Tarim Block in NW China. *Gondwana Res.* 23 (4), 1306–1315. doi:10.1016/j.gr.2012.05.009
- Zhang, F.-Q., Dilek, Y., Cheng, X.-G., Wu, H.-X., Lin, X.-B., and Chen, H.-L. (2019). Late Neoproterozoic–Early Paleozoic Seismic Structure–Stratigraphy of the SW Tarim Block (China), its Passive Margin Evolution and the Tarim–Rodinia Breakup. *Precambrian Res.* 334, 105456. doi:10.1016/j.precamres.2019.105456
- Zhang, P. H., Chen, Z. Y., Xue, L., Bao, Y. J., and Fang, Y. (2020). The Differential Diagenetic Evolution and its Influencing Factors of Lower Cambrian Black Rock Series in the Northwestern Margin of Tarim Basin. *Acta Petrol. Sin.* 36 (11), 3463–3476. doi:10.18654/1000-0569/2020.11.13
- Zhao, Z. J., Luo, J. H., Zhang, Y. B., Wu, X. N., and Pan, W. Q. (2011). Lithofacies Paleogeography of Cambrian Sequences in the Tarim Basin. *Acta Pet. Sin.* 32 (6), 937–948. (In Chinese with English abstract).
- Zhiqian, G., and Tailiang, F. (2015). Unconformities and Their Influence on Lower Paleozoic Petroleum Reservoir Development in the Tarim Basin. *J. Petroleum Sci. Eng.* 133, 335–351. doi:10.1016/j.petrol.2015.06.015
- Zhou, X. B., Li, J. H., Fu, C. J., Li, W. S., and Wang, H. H. (2012). Discussions on the Cryogenian–Cambrian Tectonic–Sedimentary Event and Tectonic Setting of Northern Tarim Basin. *Geol. China* 39 (4), 900–910. doi:10.1016/s1876-3804(12)60034-2
- Zhu, G., Chen, F., Chen, Z., Zhang, Y., Xing, X., Tao, X., et al. (2016). Discovery and Basic Characteristics of High-Quality Source Rocks Found in the Yuertusi Formation of the Cambrian in Tarim Basin, China. *J. Nat. Gas Geoscience* 1 (1), 21–33. doi:10.1016/j.jnggs.2016.05.002
- Zhu, G., Chen, F., Wang, M., Zhang, Z., Ren, R., and Wu, L. (2018). Discovery of the Lower Cambrian High-Quality Source Rocks and Deep Oil and Gas Exploration Potential in the Tarim Basin, China. *Bulletin* 102 (10), 2123–2151. doi:10.1306/03141817183
- Zhu, W., Zhang, Z., Shu, L., Lu, H., Su, J., and Yang, W. (2008). SHRIMP U–Pb Zircon Geochronology of Neoproterozoic Korla Mafic Dykes in the Northern Tarim Block, NW China: Implications for the Long-Lasting Breakup Process of Rodinia. *J. Geol. Soc.* 165 (5), 887–890. doi:10.1144/0016-76492007-174

**Conflict of Interest:** Author KD is employed by CNPC, XG is employed by CNPC, NF is employed by CNPC, LK is employed by CNPC and author WY is employed by SINOPEC.

The remaining authors declare that the research was conducted in the absence of any commercial or financial relationships that could be construed as a potential conflict of interest.

The reviewer RW declared a shared affiliation with the author WY to the handling editor at the time of review.

**Publisher's Note:** All claims expressed in this article are solely those of the authors and do not necessarily represent those of their affiliated organizations, or those of the publisher, the editors, and the reviewers. Any product that may be evaluated in this article, or claim that may be made by its manufacturer, is not guaranteed or endorsed by the publisher.

Copyright © 2022 Yuan, Chen, Dai, Guo, Kong, Feng, Zhao and Yang. This is an open-access article distributed under the terms of the Creative Commons Attribution License (CC BY). The use, distribution or reproduction in other forums is permitted, provided the original author(s) and the copyright owner(s) are credited and that the original publication in this journal is cited, in accordance with accepted academic practice. No use, distribution or reproduction is permitted which does not comply with these terms.